PERGAMON

International Journal of Solids and Structures 37 (2000) 6499–6516

INTERNATIONAL JOURNAL OF SOLIDS and STRUCTURES

www.elsevier.com/locate/ijsolstr

Determination of constitutive properties of thin metallic films on substrates by spherical indentation using neural networks

N. Huber[a,*], I. Tsagrakis[b], Ch. Tsakmakis[a,c]

[a]*Forschungszentrum Karlsruhe, Institut für Materialforschung II (IMF II), Postfach 3640, D-76021 Karlsruhe, Germany*
[b]*Laboratory of Mechanics and Materials, Aristotle University of Thessaloniki, GR-54006 Thessaloniki, Greece*
[c]*Technische Universität Darmstadt, Institut für Mechanik 1, Hochschulstrasse 1, D-64289 Darmstadt, Germany*

Received 16 February 1999; in revised form 14 September 1999

Abstract

The indentation test has been developed into a popular method for investigating mechanical properties of thin films. However, there exist only some empirical or semi-analytical methods for determining the hardness and Young's modulus of a film from pyramidal indentation of the film on a substrate, where the deformation of film and substrate is subjected to be elastic–plastic. The aim of the present paper is to show how constitutive properties and material parameters may be determined by using a depth-load trajectory which is related to a fictitious *bulk film* material. This bulk film material is supposed to possess the same mechanical properties as the real film. It is assumed that the film and the substrate exhibit elastic–plastic material properties with nonlinear isotropic and kinematic hardening. The determination of the depth-load trajectory of the bulk film is a so-called inverse problem. This problem is solved in the present paper using both the depth-load trajectory of the pure substrate and the depth-load trajectory of the film deposited on this substrate. For this, use is made of the method of neural networks. Having established the bulk film depth-load trajectory, the set of material parameters entering in the constitutive laws may be determined by using e.g. the method proposed by Huber and Tsakmakis (Huber, N., Tsakmakis, Ch., 1999. Determination of constitutive properties from spherical indentation data using neural networks. Part II: plasticity with nonlinear isotropic and kinematic hardening. J. Mech. Phys. Solids 47, 1589–1607).

Keywords: Constitutive properties; Metallic films; Neural networks

* Corresponding author. Tel.: +49-0-7247-824895; fax: +49-0-7247-822347.
E-mail address: norbert.huber@imf.fzk.de (N. Huber).

0020-7683/00/$ - see front matter
PII: S0020-7683(99)00270-X

1. Introduction

It is well known that the indentation test can be employed to obtain mechanical properties of materials. Tabor (1951) and Atkins and Tabor (1965) have shown that either a spherical indenter or several pyramidal indenters with different tip angles have to be used, when mechanical properties like the strain–stress relation are to be investigated. For example, one can determine Young's modulus (see e.g. Doerner and Nix, 1986; Pharr et al., 1992; Field and Swain, 1993; Huber et al., 1997), the hardening behavior according to monotonic loading (Meyer, 1908; Tabor, 1951; Field and Swain, 1993; Jayaraman et al., 1998), viscosity effects (Yu et al., 1986; Mayo and Nix, 1988; Raman and Berriche, 1992) and, as shown recently, the parameters governing the response of nonlinear isotropic and kinematic hardening of Armstrong Frederick type (Huber and Tsakmakis, 1999b). Note that all these methods are concerned with bulk material only.

Analytical solutions in the literature for coating/substrate systems are restricted to small elastic deformations and resulting integral equations have to be solved numerically in most cases. Yu et al. (1990) discussed the effect of the substrate on the layer/substrate stiffness for arbitrary indenter profiles. Li and Chou (1997) derived a semi-analytical solution for a spherical profile on a coating/substrate system and discussed the loading response for the cases of hard/soft and soft/hard system. However, as it has been shown by Huber et al. (1997) for bulk elastic–plastic materials and large penetrations, the determination of Young's modulus using elastic solutions will result an error depending on the hardening properties of the material.

Generally, if the mechanical properties of thin films on substrates have to be investigated, the methods developed for bulk materials have to be extended appropriately. For example, when pyramidal geometries like Vickers or Berkovich indenters are used, one can obtain the mechanical properties of the film by fitting the measured data (hardness or Young's modulus plotted against the indentation depth) with analytical solutions (Gao et al., 1992) or empirical functions (Bhattacharya and Nix, 1988; Menčik et al., 1997). The hardness or Young's modulus of the film is one of the fit parameters in the function and is determined by least square optimization. The influence of the roughness can be diminished by a large number of measurements at the same depth, using statistical methods. This procedure needs geometric similar indents which, however, allow only to determine the hardness and Young's modulus of the material with a single geometry.

The purpose of the present paper is to demonstrate how elastic and plastic properties of thin films on substrates may be determined. To this end a method is developed which may be sketched as follows. The direct problem of calculating the indentation depth-load trajectory of bulk materials or of a film on a substrate for given elasticity and hardening properties can be carried out using the Finite Element method (see Fig. 1, continuous lines). On the other hand, one may consider the problem where the depth-load trajectory according to spherical indentation is known and the material parameters in the constitutive laws are sought. Huber and Tsakmakis (1999a, 1999b) solved this so-called inverse problem for the case of bulk material exhibiting nonlinear isotropic and kinematic hardening by using neural networks. This is denoted in Fig. 1 as box IP1. In this figure, h is the indentation depth, $P(h)$ is the

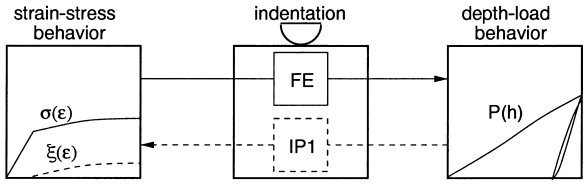

Fig. 1. Direct problem (box FE) and inverse problem (box IP1) for the indentation of a bulk material.

corresponding load, ε is the uniaxial logarithmic strain, $\sigma(\varepsilon)$ is the corresponding uniaxial true stress and $\xi(\varepsilon)$ is the corresponding uniaxial backstress.

The method can be extended to investigate the properties of thin films on substrates as shown in Fig. 2. We suppose the depth-load behavior $\bar{P}(h)$ for pure substrate material as well as the depth-load behavior $\hat{\bar{P}}(h)$ of the composite thin film — substrate to be known. To these data it is possible to assign a depth-load behavior $\hat{P}(h)$ for the (pure) bulk film material. The operator, which enables the assignment is the solution of a second inverse problem denoted as box IP2 in Fig. 2. After establishing the depth-load trajectory $\hat{P}(h)$, the constitutive parameters can be obtained as solution of an inverse problem of type 1.

2. Constitutive equations (finite deformations)

We assume elastic–plastic constitutive properties for both, the substrate and the film material. In particular, the same type of finite deformation plasticity laws, but with different material parameters, are assumed to apply. This type of constitutive equations was used in previous works as well (see Huber and Tsakmakis, 1999b) and read as follows:

$$\overset{\triangledown}{\mathbf{S}} = \dot{\mathbf{S}} - \mathbf{L}\mathbf{S} - \mathbf{S}\mathbf{L}^{\mathrm{T}} = \mathscr{C}\big[\mathbf{D} - \mathbf{D}_p\big], \tag{1}$$

$$F(t) = \bar{F}(\mathbf{S}, \boldsymbol{\xi}, k) = \sqrt{\frac{3}{2}(\mathbf{S} - \boldsymbol{\xi})^{\mathrm{D}} \cdot (\mathbf{S} - \boldsymbol{\xi})^{\mathrm{D}}} - k, \tag{2}$$

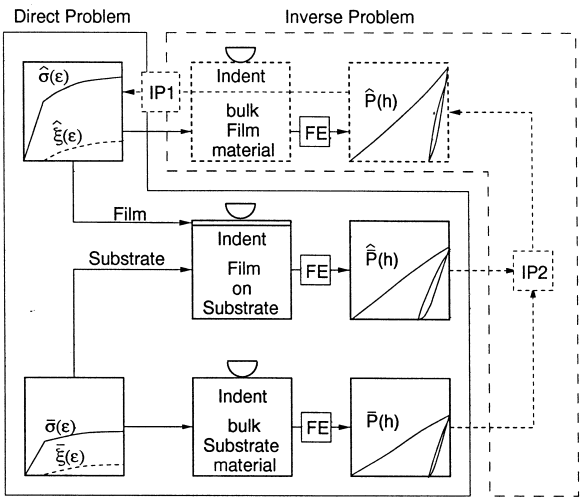

Fig. 2. Sketch of the concept to solve the inverse problem.

$$\mathbf{D}_p = \dot{s}\sqrt{\frac{3}{2}}\frac{(\mathbf{S}-\boldsymbol{\xi})^{\mathrm{D}}}{\|(\mathbf{S}-\boldsymbol{\xi})^{\mathrm{D}}\|}, \tag{3}$$

$$\dot{k} = \big(\gamma - \beta(k-k_0)\big)\dot{s}, \tag{4}$$

$$\overset{\nabla}{\boldsymbol{\xi}} = \dot{\boldsymbol{\xi}} - \mathbf{L}\boldsymbol{\xi} - \boldsymbol{\xi}\mathbf{L}^{\mathrm{T}} = c\mathbf{D}_p - b\dot{s}\boldsymbol{\xi}, \tag{5}$$

$$\dot{s} = \sqrt{\mathbf{D}_p \cdot \mathbf{D}_p}\begin{cases} > 0 & \text{for } F = 0 \;\&\; L = \big[\dot{F}\big]_{\mathbf{F}_p=\text{const}} > 0 \\ = 0 & \text{otherwise} \end{cases}. \tag{6}$$

In Eq. (1), bold-face capital letters denote second-order tensors while $\mathscr{C}$ is the fourth-order isotropic tensor:

$$\mathscr{C} = \frac{E}{1+\nu}\mathscr{E} + \frac{E\nu}{(1+\nu)(1-2\nu)}\mathbf{1}\otimes\mathbf{1}. \tag{7}$$

Here, E denotes Young's modulus, ν is Poisson ratio, while $\mathscr{E}$ and $\mathbf{1}$ are the identity tensors of fourth- and second-order, respectively. In the following, the value of ν is assumed to be given by 0.3. The symbol $\otimes$ denotes the dyadic (tensor) product. Further, $\mathbf{A}^{\mathrm{D}}$ and $\mathbf{A}^{\mathrm{T}}$ represent the deviator and the transpose of the second order tensor $\mathbf{A}$, respectively, $\mathbf{A}\cdot\mathbf{B}$ is the usual inner product between the second order tensors $\mathbf{A}$ and $\mathbf{B}$ and $\|\mathbf{A}\|$ is Euclidean norm of $\mathbf{A}$, i.e. $\|\mathbf{A}\| = \sqrt{\mathbf{A}\cdot\mathbf{A}}$. The quantity $\mathbf{S}$ denotes Cauchy stress tensor and $\boldsymbol{\xi}$ is the back-stress tensor. Moreover, $\mathbf{L}$ is the spatial velocity gradient with symmetric part $\mathbf{D} = \frac{1}{2}(\mathbf{L}+\mathbf{L}^{\mathrm{T}})$ and s is the arclength of plastic deformation. The scalar variable $\dot{s}$ has to be determined from the so-called consistency condition $\dot{F} = 0$. Eqs. (4) and (5) represent the laws governing isotropic and kinematic hardening, respectively, the variable responsible for isotropic hardening being denoted by k. Finally, k_0, γ, β, c and b denote material parameters.

The constitutive equations (1)–(6) have been incorporated as a user supplied subroutine into the Finite Element code ABAQUS. The integration algorithm used for the local iterations is based on the method of Hughes and Winget (1980) as well as the method of elastic predictor — plastic corrector (for more details see Diegele et al., 1998).

Note that instead of the plasticity law (1)–(6) other type of constitutive equation like those e.g. derived on the basis of the scale invariance approach (Aifantis, 1987, 1995) can also be employed but this issue may be taken up in a future study.

It can be shown that for uniaxial tension loading, Eqs. (2), (4) and (5) imply

$$\sigma = S_{11} = k + \xi, \tag{8}$$

with

$$k = k_0 + \frac{\gamma}{\beta}(1 - \mathrm{e}^{-\beta s}), \tag{9}$$

$$\xi = \xi_{11} - \xi_{22} = \frac{c}{b-2}\big(1 - \mathrm{e}^{-(b-2)s}\big) + \frac{c}{2(b+1)}\big(1 - \mathrm{e}^{-(b+1)s}\big). \tag{10}$$

In these equations, we write A_{11} for the uniaxial component of a second-order tensor $\mathbf{A}$. Characteristic properties of the hardening behavior may be represented by the stress $\Delta\Sigma$ defined by

$$\Delta\Sigma := \lim_{s\to\infty} \sigma - k_0 = \frac{\gamma}{\beta} + \frac{3}{2}\frac{c}{b} f(b), \tag{11}$$

$$f(b) = \frac{b^2}{b^2 - b - 2}. \tag{12}$$

Of course, when characterizing hardening properties, one may omit the nonlinear function $f(b)$ in Eq. (11). Thus, in what follows we will use the stresses

$$\Delta\sigma := \frac{\gamma}{\beta} + \frac{3}{2}\frac{c}{b}, \tag{13}$$

$$\Delta\xi := \frac{3}{2}\frac{c}{b} \tag{14}$$

and the moduli

$$\sigma' := \lim_{s\to 0} \frac{\mathrm{d}\sigma}{\mathrm{d}s} = \gamma + \frac{3}{2}c, \tag{15}$$

$$\xi' := \lim_{s\to 0} \frac{\mathrm{d}\xi}{\mathrm{d}s} = \frac{3}{2}c \tag{16}$$

Also, it is convenient to introduce the vector of material parameters

$$\mathbf{q} := (E, k_0, \gamma, \beta, c, b). \tag{17}$$

3. Neural networks

Artificial neural networks represent a qualified tool for solving complex inverse problems in computational mechanics. An overview about some relevant applications is given by Yagawa and Okuda (1996) and Sumpter and Noid (1996). As outlined by Huber and Tsakmakis (1999a), a neural network consists of neurons connected with links to a highly parallel structure. Each neuron possesses a

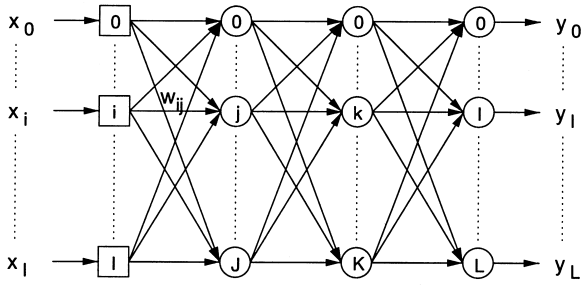

Fig. 3. Sketch of a multilayer feed forward neural net.

local memory and can carry out localized information processing operations. In general, each neuron has multiple inputs and a single output value to mimic the biological brain neuron.

Presenting training patterns to the network, which consists of the input values x_i and the related desired output values d_l, the error for each pattern can be computed from the actual output y_l (see Fig. 3). Using a backpropagation algorithm, the synaptic weights w_{ij}, which represent the links between the neurons are adjusted appropriately. Thus, the error of the output values is minimized and the network has been taught the relation between input and output values.

The neural network simulations are carried out using the SNNS (1995) code. The relevant theory of backpropagation and preparation of the data in the present context is described by Huber and Tsakmakis (1999a, 1999b).

4. Determination of material properties for bulk materials

The neural networks used by Huber and Tsakmakis (1999b), representing the operator IP1 in Fig. 2, are functions able to determine the material parameters from a given depth-load trajectory of a bulk material. They have been implemented in the program INDENTIFY which extracts the necessary data from the measured depth-load response, generates the input data, calls the neural networks and calculates the sought material parameters. This method is able to determine the constitutive properties for bulk materials only in the present state. Three types of input data from the depth-load response has to be provided to INDENTIFY (see Fig. 4).

The first type of input data is represented by the loading response $P_l(h)$ which contains information about the sum of isotropic and kinematic hardening, i.e. the monotonic strain–stress response. The second type of input data is the unloading stiffness $S:=\mathrm{d}P_u/\mathrm{d}h|_{h_t}$ at the beginning of an unloading, which is related to the elastic properties of the material. The third type of input data is the hysteresis geometry, which results from an unloading reloading cycle and indicates the kinematic hardening response. It has been shown by Huber and Tsakmakis (1999a), that the hysteresis geometry can be described conveniently with the dimensionless quantities for the opening along the load axis (see Fig. 4)

$$\Delta P^* := \frac{\Delta P}{P_t} = \frac{P_r(h) - P_u(h)}{P_t}, \quad h \in [h_r, h_t] \tag{18}$$

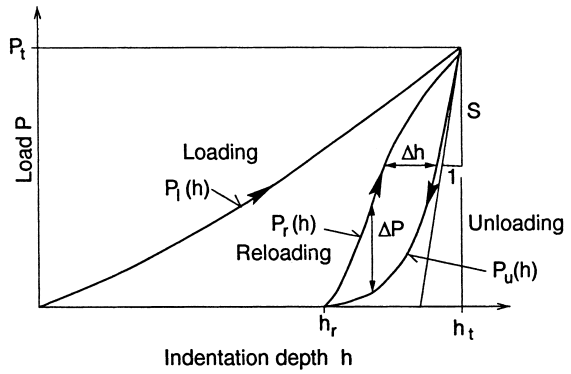

Fig. 4. Sketch of the depth-load trajectory for cyclic indentation.

and the width along the depth axis

$$\Delta h^* := \frac{\Delta h}{h_t} = \frac{h\left(P_u^* = P^*\right) - h\left(P_r^* = P^*\right)}{h_t}, \tag{19}$$

where $h(P_u^* = P^*)$ is the unloading depth and $h(P_r^* = P^*)$ is the reloading depth at a given load $P^* := P/P_t$. The input data for the neural networks are defined to be values $P_l(h^* := h/R)$ and $\Delta P^*(\delta^* := (h - h_r)/(h_t - h_r))$ for some h^* and δ^*, respectively, as well as $\Delta h^*(P^* := P/P_t)$ for some P^*.

The input data of the loading response are

$$P_{l,i} = P_l\left(h_i^*\right), \tag{20}$$

with

$$h_i^* = \left\{6.25 \cdot 10^{-4}, 1.25 \cdot 10^{-3}, 2.5 \cdot 10^{-3}, 5 \cdot 10^{-3}, 0.01, 0.02, 0.04, 0.06\right\}, \quad 1 \le i \le 8. \tag{21}$$

The hysteresis loops may be inserted in the range $0.02 \le h_t^* \le 0.1$. In the present work, five hysteresis loops at

$$h_{t,i}^* = \{0.02, 0.04, 0.06, 0.08, 0.1\}, \quad 1 \le i \le 5 \tag{22}$$

were inserted. As outlined by Huber and Tsakmakis (1999a), the hysteresis loops for these h_t-values do not effect the form of the loading response. In other words, the values $P_{l,\,i}$ for $i = 6, 7, 8$ are the same as if no hysteresis loops would have been inserted. The data for the hysteresis needed are

$$\Delta P_i^* = \Delta P^*\left(\delta_i^*\right), \tag{23}$$

$$\delta_i^* = \{0.25, 0.5, 0.75\}, \; 1 \le i \le 3, \tag{24}$$

$$\Delta h_i^* = \Delta h^*\left(P_i^*\right), \tag{25}$$

$$P_i^* = \{0.25, 0.5, 0.75\}, \; 1 \le i \le 3. \tag{26}$$

In order to determine the material parameters $\hat{\mathbf{q}}$ of the film with INDENTIFY, the above values of the loading response, of the hysteresis loop and in addition, of the unloading stiffness have to be known for the bulk film material. As mentioned in Section 1, the bulk film material is a fictitious material, which has the same elasticity and hardening properties as the real film material (see dashed lines in Fig. 2).

5. Spherical indentation of films on substrates

Let us denote P and R be the force acting on the sphere and the radius of the sphere, respectively, and let h be the indentation depth. The thickness of the film will be denoted by t. Further, let us consider a loading history consisting of loading until $h = h_t$, $P = P_t$, unloading until $P = 0$ with $h = h_r$, and reloading until $h = h_t$ (see Fig. 4). Note in passing, that beside the radius of the indenter R, the film thickness t is another characteristic length of the problem in the case of a film on a substrate (see Fig. 5).

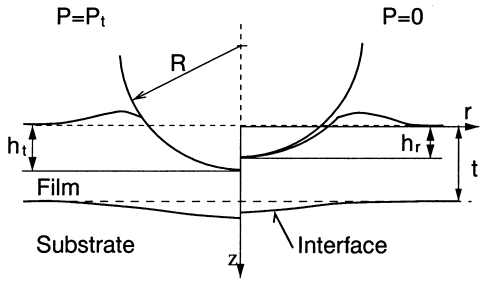

Fig. 5. Geometry of spherical indentation of a film on a substrate.

5.1. Finite element simulations

All Finite Element calculations performed in this work are based on the Finite Element mesh with eight-node axisymmetric elements, described in detail elsewhere (see Huber and Tsakmakis, 1998). However, this mesh is slightly modified, in order to insert the film on the top. The modified mesh is displayed in Fig. 6.

The number of relevant material parameters for the creation of the training patterns is six for each material, namely (E, k_0, γ, β, c, b). As mentioned previously, the Poisson ratio ν is supposed to be constant $\nu = 0.3$ in the present paper. For all Finite Element simulations, the radius of the spherical indenter and the thickness of the film are chosen to be $R = 5$ mm and $t = 1.12$ mm, respectively. Thus, our calculations are based on the fixed ratio $t/R = 0.224$. For a maximum indentation depth of

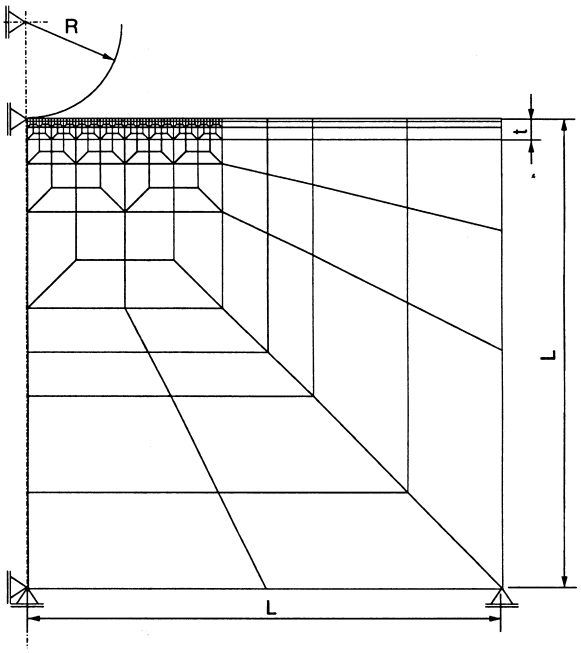

Fig. 6. Finite Element mesh for spherical indentation of a film on a substrate.

Table 1
Parameter basis for the film and substrate material used in the finite element simulations

Parameter	Range
E (GPa)	100.0, 200
k_0 (MPa)	50.0–300
$\Delta\sigma/k_0$ (-)	0.2–300
$\gamma/(\beta\Delta\sigma)$ (-)	0.0–1.0
γ (GPa)	3.0–30
c (GPa)	2–20

$h/R = 0.1$, the indenter penetrates almost half of the film thickness which requires to deal with geometrical nonlinear theories.

As outlined by Huber and Tsakmakis (1999b), for keeping the number of necessary simulations small, the parameters (E, k_0, γ, β, c, b) have to be chosen randomly from the given intervals. For the purpose of the present study, these intervals are defined as in Table 1. In the following, the symbol (-) is used to denote non-dimensional quantities with no scaling.

It remains to develop a method for assigning a depth-load trajectory of the bulk film material to given depth-load trajectories of the composite (film on substrate) and the substrate. This will be done in the following for the loading responses and the hysteresis loops separately.

5.2. Loading response

The load for the composite $\hat{\bar{P}}_l$ (film on substrate) at a depth h is dependent on the material parameters of the film $\hat{\mathbf{q}}_l = (\hat{E}, \hat{k}_0, \hat{\sigma}', \Delta\hat{\sigma})$, the material parameters of the substrate $\bar{\mathbf{q}}_l = (\bar{E}, \bar{k}_0, \bar{\sigma}', \Delta\bar{\sigma})$ and the geometry:

$$\hat{\bar{P}}_l = \hat{\bar{\mathscr{P}}}_l\big(\hat{\mathbf{q}}_l, \bar{\mathbf{q}}_l, R, t, h\big). \tag{27}$$

The function $\hat{\bar{\mathscr{P}}}_l$ in Eq. (27) is given implicitly by calculating the values of $\hat{\bar{P}}_l$ at prescribed points ($\hat{\mathbf{q}}_l$, $\bar{\mathbf{q}}$, R, t, h) via Finite Element simulations.

Similarly, for the bulk film material and bulk substrate material, the relations

$$\hat{P}_l = \hat{\mathscr{P}}_l\big(\hat{\mathbf{q}}_l, R, h\big) \tag{28}$$

and

Table 2
Input- and output-data for LoadNet

Inputs x_i					
$\frac{\hat{\bar{P}}_{l,i}}{\bar{P}_{l,i}}\, i = 1,\ldots,8$	$\frac{\hat{\bar{P}}_{l,i}}{\hat{\bar{P}}_{l,8}}\quad i = 1,\ldots,7$	$\frac{\bar{P}_{l,i}}{\bar{P}_{l,8}}\, i = 1,\ldots,7$	$\frac{h_t}{R}$	$\frac{\hat{\bar{P}}_t}{\bar{P}_t}$	$\frac{\hat{\bar{S}}(h_t)}{\bar{S}(h_t)}$
Outputs y_l					
$\frac{\hat{P}_{l,i}}{\hat{P}_{l,i}^{(\mathrm{est})}}\, i = 1,\ldots,8$	$\frac{\hat{P}_t}{\hat{P}_t^{(\mathrm{est})}}$	$\frac{\hat{S}(h_t)}{\bar{S}(h_t)}$			

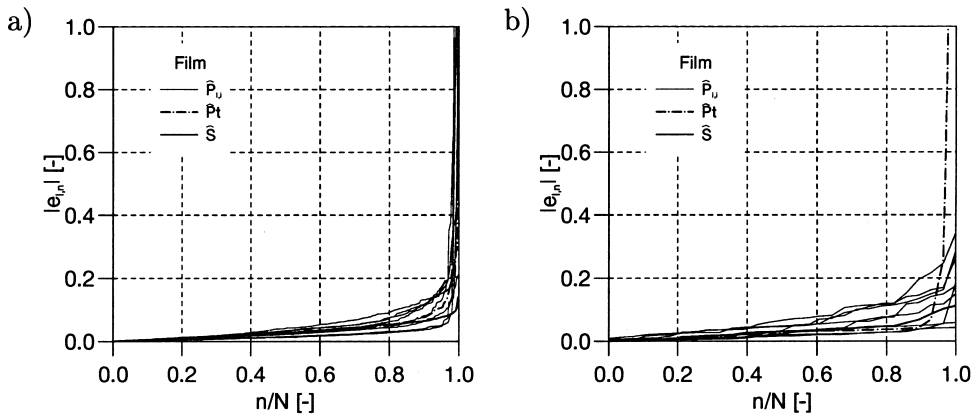

Fig. 7. Error distributions for $\hat{P}_{l,i}$, $\hat{P}_t$ and $\hat{S}$: (a) Number of the training patterns $N = 346$, (b) Number of the test patterns $N = 29$.

$$\bar{P}_l = \bar{\mathscr{P}}_l(\bar{\mathbf{q}}_l, R, h) \tag{29}$$

hold, respectively.

Evidently, the unloading stiffnesses at $h = h_t$ for the composite, the bulk film and the bulk substrate material satisfy equations of the form

$$\hat{\bar{S}} = \hat{\bar{\mathscr{S}}}_l(\hat{\mathbf{q}}_l, \bar{\mathbf{q}}_l, R, t, h_t), \tag{30}$$

$$\hat{S} = \hat{\mathscr{S}}_l(\hat{\mathbf{q}}_l, R, h_t), \tag{31}$$

$$\bar{S} = \bar{\mathscr{S}}_l(\bar{\mathbf{q}}_l, R, h_t), \tag{32}$$

respectively.

Now suppose that values $\hat{P}_{l,i}$, $\bar{P}_{l,i}$ at points h_i, $i = 1, \ldots, n$, as well as values $\hat{S}$, $\bar{S}$, at h_t are given. For these values, we assume that Eqs. (28) and (31) as well as Eqs. (29) and (32) can be solved for $\hat{\mathbf{q}}_l$ and $\bar{\mathbf{q}}_l$, respectively, to give

$$\hat{\mathbf{q}}_l = \hat{Q}_l\left(h_i, \hat{P}_{l,i}, \hat{S}, R, h_t\right), \tag{33}$$

$$\bar{\mathbf{q}}_l = \bar{Q}_l(h_i, \bar{P}_{l,i}, \bar{S}, R, h_t). \tag{34}$$

In the following, we set $n = 8$, the values $h_1, \ldots, h_8$ being given in Eq. (21). For h_t^* (respectively h_t) one may use one of the values given in Eq. (22). Thus, the values h_i being chosen fixed, Eqs. (33) and (34) may be rewritten as

$$\hat{\mathbf{q}}_l = \hat{Q}_l\left(\hat{P}_{l,i}, \hat{S}, R, h_t\right), \tag{35}$$

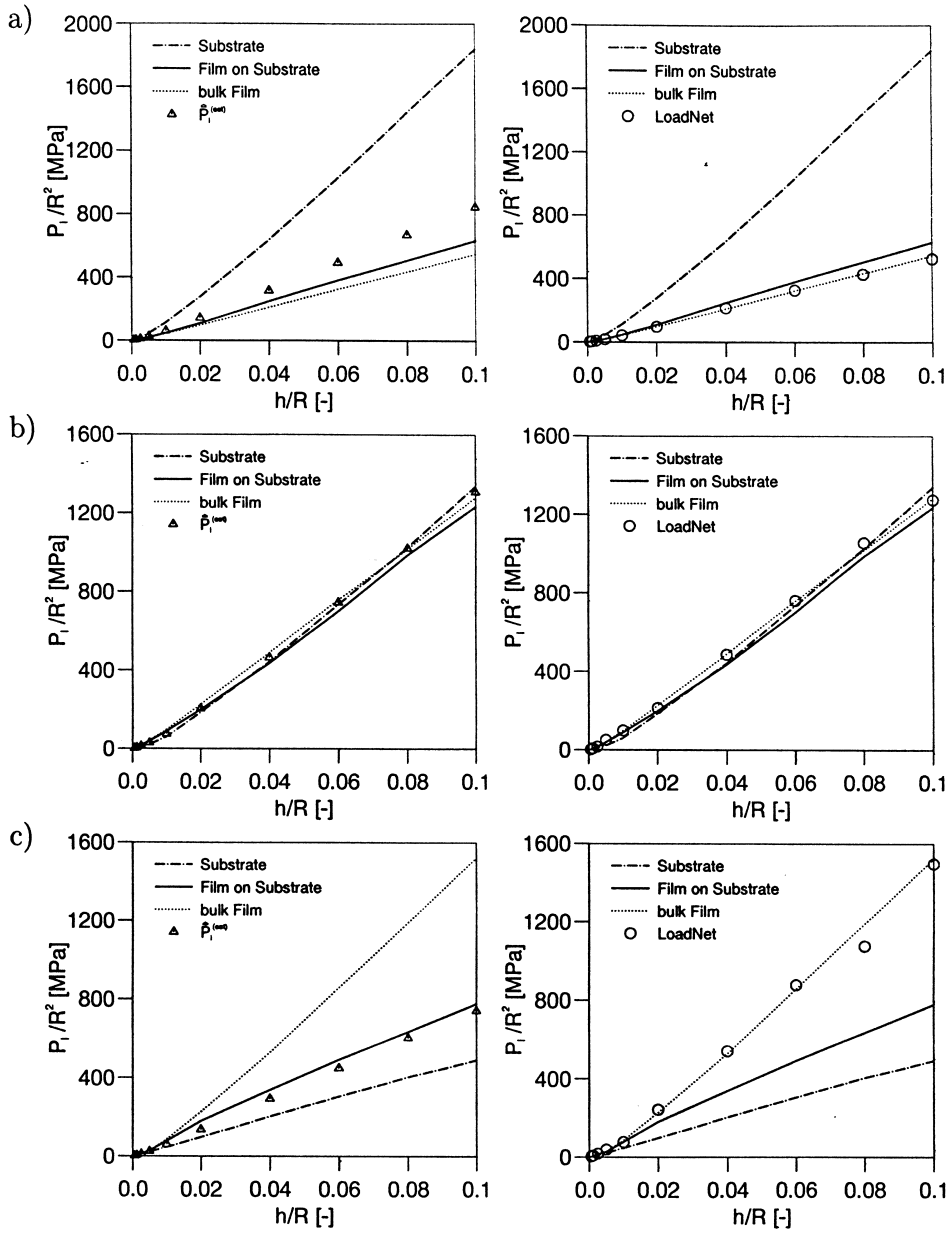

Fig. 8. Some test examples of loading responses: (a) soft film on hard substrate; (b) approximately same hardness; (c) hard film on soft substrate. Light-hand side: $\hat{P}_l^{(est)}$ values for given responses of film and substrate. Right-hand side: determination of the bulk film response using LoadNet.

Table 3
Input- and output-data for HystNet

Inputs x_i									
$\frac{\hat{\bar{P}}_{l,i}}{\hat{\bar{P}}_{l,8}} i = 4,\ldots,7$	$\frac{\bar{P}_{l,i}}{\bar{P}_{l,8}} i = 4,\ldots,7$	$\frac{\hat{\bar{P}}_{l,8}}{\bar{P}_{l,8}}$	$\frac{h_t}{R}$	$\frac{\hat{\bar{P}}_t}{\bar{P}_t}$	$\frac{\hat{\bar{S}}(h_t)}{\bar{S}(h_t)}$	$\frac{\Delta\hat{\bar{P}}_1}{\Delta\hat{\bar{P}}_2}$	$\frac{\Delta\hat{\bar{P}}_2}{\hat{\bar{P}}_t}$	$\frac{\Delta\hat{\bar{P}}_3}{\Delta\hat{\bar{P}}_2}$	$\frac{\Delta\bar{P}_1}{\Delta\bar{P}_2}$
$\frac{\Delta\bar{P}_2}{\bar{P}_t}$	$\frac{\Delta\bar{P}_3}{\Delta\bar{P}_2}$	$\frac{\Delta\hat{\bar{P}}_2}{\Delta\bar{P}_2}$	$\frac{\Delta\hat{\bar{h}}_1}{\Delta\hat{\bar{h}}_2}$	$\frac{\Delta\hat{\bar{h}}_2}{h_t}$	$\frac{\Delta\hat{\bar{h}}_3}{\Delta\hat{\bar{h}}_2}$	$\frac{\Delta\bar{h}_1}{\Delta\bar{h}_2}$	$\frac{\Delta\bar{h}_2}{h_t}$	$\frac{\Delta\bar{h}_3}{\Delta\bar{h}_2}$	$\frac{\Delta\hat{\bar{h}}_2}{\Delta\bar{h}_2}$
Outputs y_l									
$\frac{\Delta\hat{P}_1}{\Delta\hat{\bar{P}}_2}$	$\frac{\Delta\hat{P}_2}{\Delta\hat{\bar{P}}_2}$	$\frac{\Delta\hat{P}_3}{\Delta\hat{\bar{P}}_2}$	$\frac{\Delta\hat{h}_1}{\Delta\hat{\bar{h}}_2}$	$\frac{\Delta\hat{h}_2}{\Delta\hat{\bar{h}}_2}$	$\frac{\Delta\hat{h}_3}{\Delta\hat{\bar{h}}_2}$				

$$\bar{\mathbf{q}}_l = \bar{Q}_l(\bar{P}_{l,i}, \bar{S}, R, h_t), \tag{36}$$

respectively. On substituting Eqs. (35) and (36) in Eq. (27), we obtain for $\hat{\bar{P}}_l$ a relation of the form

$$\hat{\bar{P}}_{l,i} = \hat{\bar{\Pi}}\left(\hat{P}_{l,i}, \bar{P}_{l,i}, \hat{S}, \bar{S}, R, h_t\right) \tag{37}$$

For given loading responses and unloading stiffnesses of the composite and the substrate, respectively, one obtains analogous

$$\hat{P}_{l,i} = \hat{\Pi}\left(\hat{\bar{P}}_{l,i}, \bar{P}_{l,i}, \hat{\bar{S}}, \bar{S}, R, h_t\right), \tag{38}$$

where the arguments of $\hat{\Pi}$ represent the necessary inputs of the neural networks to be developed.

In order to obtain neural networks appropriate for arbitrary indenter radii, the input- and output quantities must be given in dimensionless form. Generally, to define dimensionless quantities in a form suitable to the neural network is a matter of experience. It has been turned out, that the best results are achieved for the dimensionless input and output quantities given in Table 2. The quantity $\hat{P}_{l,i}^{(\mathrm{est})}$ in Table 2 is defined by

$$\hat{P}_{l,i}^{(\mathrm{est})} = \hat{P}_l^{(\mathrm{est})}(h_i), \tag{39}$$

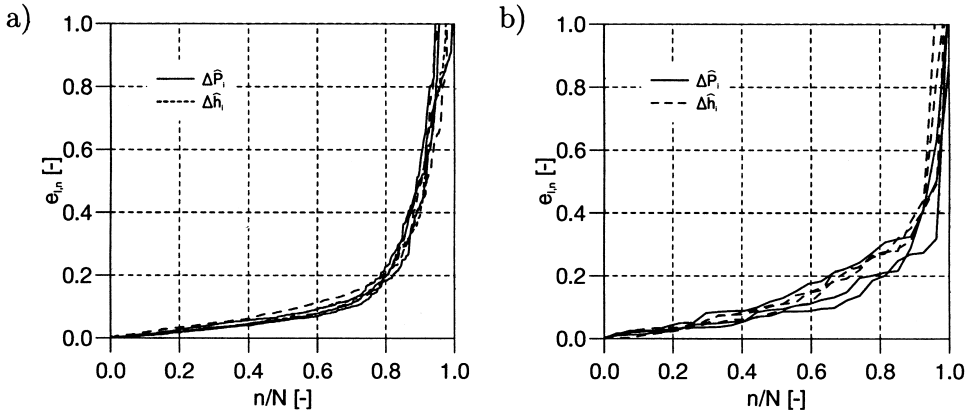

Fig. 9. Error distribution for the bulk film hysteresis $\Delta\hat{P}_i$ and $\Delta\hat{h}_i$: (a) Number training patterns $N = 324$; (b) Number of test patterns $N = 28$.

Table 4
Used and identified parameter sets for test example in Figs. 8(a) and 11(a)

S[a]/F[b]/I[c]	h_i^* (-)	E (GPa)	k_0 (MPa)	σ' (MPa)	$\Delta\sigma$ (MPa)	ξ' (MPa)	$\Delta\xi$ (MPa)
S	–	200	369	43897	1064	24525	142
F	–	100	107	29729	186	15894	64
I	0.02	91	138	15100	164	9300	60
I	0.04	107	132	13800	177	7727	64
I	0.06	107	130	13710	183	7083	70
I	0.08	103	131	15250	175	7336	72
I	0.10	93	135	17860	166	9010	68

[a] S: Substrate.
[b] F: Film.
[c] I: Identified.

where

$$\hat{P}_l^{(\mathrm{est})} = \frac{\hat{\bar{P}}_l \bar{P}_l}{2\bar{P}_l - \hat{\bar{P}}_l}. \tag{40}$$

To motivate Eq. (40) we suppose the values of $\bar{P}_l$ and $\hat{P}_l$ at a given h to be known. Then, a corresponding value for $\hat{\bar{P}}_l$ at the same h can be estimated by the formula

$$\hat{\bar{P}}_l^{(\mathrm{est})} = \hat{P}_l\left(\frac{\bar{P}_l}{\bar{P}_l + \hat{P}_l}\right) + \bar{P}_l\left(\frac{\hat{P}_l}{\bar{P}_l + \hat{P}_l}\right) = \frac{2\bar{P}_l\hat{P}_l}{\bar{P}_l + \hat{P}_l}. \tag{41}$$

Actually, Fig. 8 shows that Eq. (41) estimates the values of $\hat{\bar{P}}_l$ appropriately. On the other hand, one can consider the values of $\bar{P}_l$ and $\hat{\bar{P}}_l$ to be known so that, from Eq. (41), the value of $\hat{P}_l$ can be estimated by Eq. (40).

A neural network, denoted as *LoadNet*, is created using the input and output data displayed in Table 2. Besides the 35 neurons corresponding to the 25 input- and the 10 output data, LoadNet possesses two hidden layers with 20 and 15 neurons, respectively.

The resulting mean error after 1000 training cycles (epoches) was 0.00047 for 346 training patterns and 0.00093 for 29 test patterns. To obtain a more detailed overview about the error distribution, the relative error $e_{l,n}$ for a given output neuron l and pattern n, defined by

$$e_{l,n} = |\frac{y_{l,n} - d_{l,n}}{d_{l,n}}|, \tag{42}$$

is plotted against the position n/N in the ascending sequence of all N values of $e_{l,n}$. For each n, the quantities $y_{l,n}$ and $d_{l,n}$ are defined as in Section 3. The resulting plots for the training and test patterns are shown in Fig. 7(a) and (b), respectively. It can be seen that about 80% of the load values have an error less than 10% and 80% of the stiffness values have an error less than 5% for training and test patterns. Some examples of determined loading responses for the bulk film using LoadNet are given in Fig. 8(a)–(c).

5.3. Hysteresis loops

It was pointed out by Huber and Tsakmakis (1999a, 1999b), that the existence of hysteresis loops in

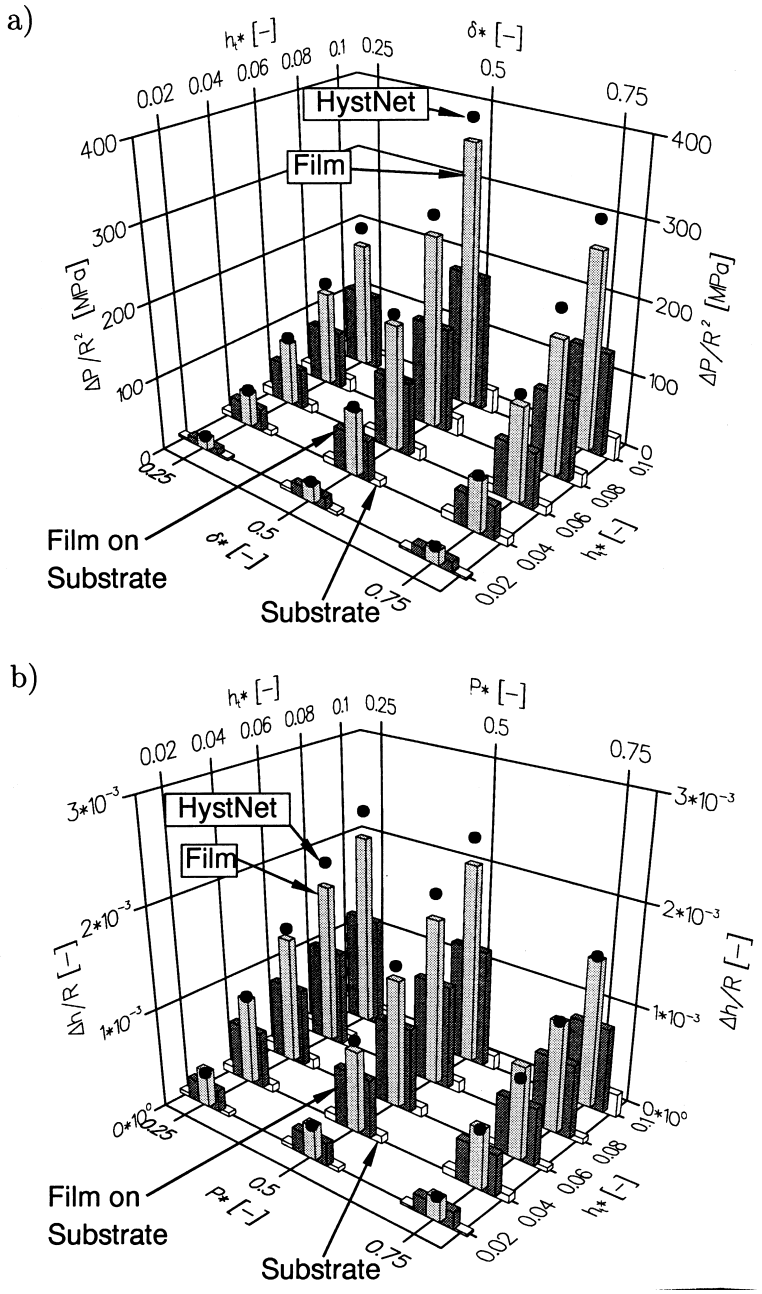

Fig. 10. Examples of identification of the bulk film hysteresis geometry using HystNet corresponding to Fig. 8(c): (a) Opening $\Delta\hat{P}_i$; (b) Width $\Delta\hat{h}_i$.

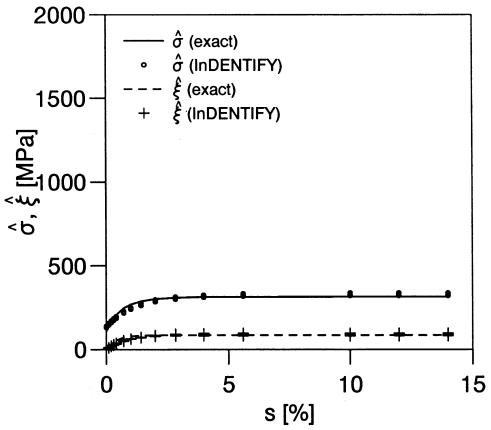

Fig. 11. $\hat{\sigma}(s)$ and $\hat{\xi}(s)$ relations identified from the bulk film depth-load trajectories using INDENTIFY. The example corresponds to the test pattern discussed in Fig. 8(a).

the depth-load trajectory indicates the existence of kinematic hardening in the material response. However, the size of the hysteresis loops depends also on Young's modulus and the isotropic hardening inherent in the material. Generally, in order to gain the hysteresis loop geometry of the bulk film material, the hysteresis loop geometries, the unloading stiffness and the loading responses of both the substrate material and the composite, are needed.

Next, we proceed to determine the hysteresis loop geometry of the bulk film material by using a neural network, which is denoted by *HystNet*. It has been turned out, that the best results with HystNet are obtained, when use is made of the dimensionless input and output data given in Table 3. The quantities $\Delta\hat{\bar{P}}_2$ and $\Delta\hat{\bar{h}}_2$, corresponding to the composite material, are defined as in Eqs. (23)–(26). According to Table 3, HystNet has 26 neurons in the input layer and six neurons in the output layer.

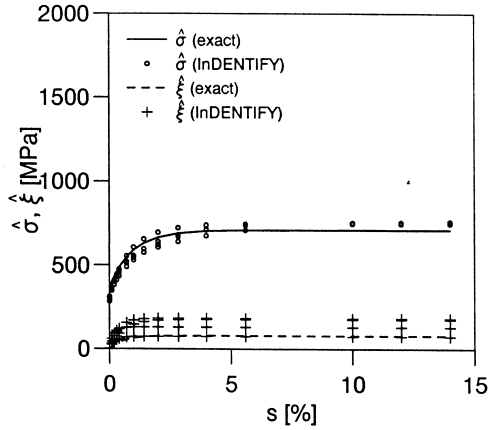

Fig. 12. $\hat{\sigma}(s)$ and $\hat{\xi}(s)$ relations identified from the bulk film depth-load trajectories using INDENTIFY. The example corresponds to the test pattern discussed in Fig. 8(b).

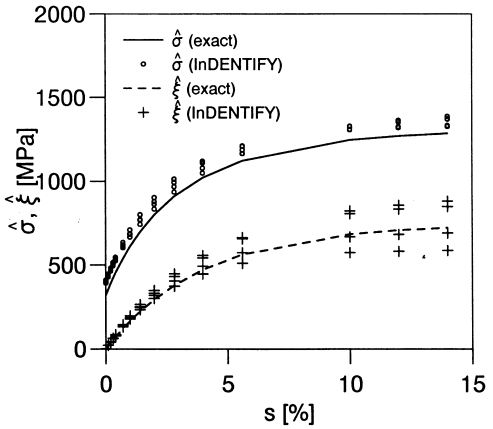

Fig. 13. $\hat{\sigma}(s)$ and $\hat{\xi}(s)$ relations identified from the bulk film depth-load trajectories using INDENTIFY. The example corresponds to the test pattern discussed in Fig. 8(c).

Additionally, two hidden layers with 18 and 10 neurons, respectively, are incorporated in HystNet. After training, the mean error was 0.00072 for 324 training patterns and 0.00165 for 28 test patterns.

Fig. 9 shows the distribution of the relative errors which are lower than 20% for 80% of the training patterns and lower than 30% for 80% of the test patterns. However, it must be noted, that the large values for the relative error are obtained for hysteresis loops with very small thickness. Nevertheless, it is discussed below that for such hysteresis loops, the identified material parameters are physically acceptable. This comes from the fact, that hysteresis loops with very small thickness are associated with vanishing small parameters in the kinematic hardening law. Consequently, large relative errors for so vanishing small material parameters cannot be physically important.

In order to demonstrate the capabilities of HystNet, Fig. 10 displays the determined opening values $\Delta\hat{P}_i/R^2$ and the determined width values $\Delta\hat{h}_i/R$ for case (c) in Fig. 8 (hard film on soft substrate). This is the most unfavorable case because of the very soft hardening behavior of the substrate material,

Table 5
Used and identified parameter sets for test example in Figs. 8(b) and 12

S[a]/F[b]/I[c]	h_i^* (-)	E (GPa)	$k0$ (MPa)	σ' (MPa)	$\Delta\sigma$ (MPa)	ξ' (MPa)	$\Delta\xi$ (MPa)
S	–	100	320	31553	784	14099	542
F	–	200	369	33399	320	9798	58
I	0.02	188	310	45540	392	23580	131
I	0.04	187	306	44280	412	36680	137
I	0.06	191	302	42800	435	22940	54
I	0.08	201	283	78720	436	60270	97
I	0.10	201	252	–	–	–	–

[a] S: Substrate.
[b] F: Film.
[c] I: Identified.

Table 6
Used and identified parameter sets for test example in Figs. 8(c) and 13

S[a]/F[b]/I[c]	h_t^* (-)	E (GPa)	k_0 (MPa)	σ'	$\Delta\sigma$	ξ' (MPa)	$\Delta\xi$ (MPa)
S	–	200	153	29077	79	9522	39
F	–	200	320	31554	784	14100	542
I	0.02	196	401	28190	777	15710	436
I	0.04	186	410	32020	748	16020	516
I	0.06	196	400	33250	763	16720	640
I	0.08	187	393	32930	786	15470	672
I	0.10	197	423	23320	755	15590	639

[a] S: Substrate.
[b] F: Film.
[c] I: Identified.

compared to the hardening behavior of the film material. From Fig. 10 it can be seen that the hysteresis geometry (opening and width) is accurately determined in the whole depth range $0.02 \leq h_t/R \leq 0.1$.

5.4. Strain–stress response

Having established the load response and the hysteresis loop geometries, the whole inverse problem is completed by applying IDENTIFY to determine $\hat{\boldsymbol{q}}$. Following the work of Huber and Tsakmakis (1999a, 1999b), several unloading–reloading cycles were inserted at the depths $h_{t,i}^*$, $i = 1, \ldots, 5$, where $h_{t,i}^*$ is defined in Eq. (22).

The results are displayed in Figs. 11–13. The circles and crosses plotted against the s-axis denote $\hat{\sigma}$ and $\hat{\xi}$ values, respectively, which differ slightly due to different hysteresis loops. As indicated in the previous section, the identification scatter increases with increasing hardness ratio, i.e. with increasing hardening characteristic of the film material and decreasing hardening characteristic of the substrate material. The results in Figs. 11–13 are related to the test examples of Fig. 8(a)–(c), respectively. For these test examples, the smallest and the largest hardness ratio corresponds to Fig. 8(a) and (c), respectively. Tables 4–6 display the used and the identified sets of parameters associated to Fig. 8(a)–(c).

Generally, from Tables 4–6 and Figs. 11–13 can be seen, that a deviation of k_0 is compensated by a corresponding change of the modulus σ'. The independency of the indentation depth shows that the neural networks LoadNet and HystNet are able to extract the film properties from the provided data in form of the bulk film depth-load trajectory.

6. Conclusions

The studies of the present paper have shown that constitutive properties of thin films as well as material parameters in constitutive models assumed to govern the response of thin films may be determined by using neural networks. The key point of the method developed is the assumption of a fictitious depth-load trajectory for the bulk film material. Calculated examples illustrate that the method proposed is able to solve the so-called inverse problem with realistic effort. Clearly, the present work has to be understood as a first step towards investigating constitutive properties of thin films on substrates.

For instance, further studies have to be carried out in order to analyze the effect, e.g. of viscosity or of intrinsic stresses.

Acknowledgements

The first author gratefully acknowledges financial support from the Hermann von Helmholtz-Gemeinschaft Deutscher Forschungszentren. Also, the encouragement and support by Professor E.C. Aifantis involving in particular the second author through the EU projects TMR #ERBFMRXCT960062 and REVISA #FI4SCT960024 is gratefully acknowledged.

References

Aifantis, E.C., 1987. The physics of plastic deformation. Int. J. Plasticity 3, 211–247.
Aifantis, E.C., 1995. From micro- to macro-plasticity: the scale invariance approach. J. Engng. Mat. Tech. 117, 352–355.
Atkins, A.G., Tabor, D.T., 1965. Plastic indentation in metals with cones. J. Mech. Phys. Solids 13, 149–164.
Bhattacharya, A.K., Nix, W.D., 1988. Analysis of elastic and plastic deformation associated with indentation testing of thin films on substrates. Int. J. Solids Structures 24, 1287–1298.
Diegele, E., Jansohn, W., Tsakmakis, Ch., 1998. Integration of finite deformation plasticity and viscoplasticity laws exhibiting nonlinear hardening rules, submitted for publication.
Doerner, M.F., Nix, W.D., 1986. A method for interpreting the data from depth-sensing indentation. J. Mater. Res. 1, 601–609.
Field, J.S., Swain, M.V., 1993. A simple predictive model for spherical indentation. J. Mater. Res. 8, 297–306.
Gao, H., Chiu, C.-H., Lee, J., 1992. Elastic contact versus indentation modeling of multi-layered materials. Int. J. Solids Structures 29, 2471–2492.
Huber, N., Munz, D., Tsakmakis, Ch., 1997. Determination of Young's modulus by spherical indentation. J. Mater. Res. 12, 2459–2469.
Huber, N., Tsakmakis, Ch., 1998. A finite element analysis of the effect of hardening rules on the indentation test. J. Eng. Mat. Tech. 120, 143–148.
Huber, N., Tsakmakis, Ch., 1999a. Determination of constitutive properties from spherical indentation data using neural networks. Part I: the case of pure kinematic hardening in plasticity laws. J. Mech. Phys. Solids 47, 1569–1588.
Huber, N., Tsakmakis, Ch., 1999b. Determination of constitutive properties from spherical indentation data using neural networks. Part II: plasticity with nonlinear isotropic and kinematic hardening. J. Mech. Phys. Solids 47, 1589–1607.
Hughes, T.J.R., Winget, J., 1980. Finite rotation effects in numerical integration of rate constitutive equations in large-deformation analysis. Int. J. Num. Meth. Eng. 15, 1862–1867.
Jayaraman, S., Hahn, G.T., Oliver, W.C., Rubin, C.A., Bastias, P.C., 1998. Determination of monotonic stress strain curve of hard materials from ultra-low-load indentation tests. Int. J. Solids Structures 35, 365–381.
Li, J., Chou, T.W., 1997. Elastic field of a thin-film/substrate system under an axisymmetric loading. Int. J. Solids Structures 34, 4463–4478.
Meyer, E., 1908. Untersuchungen über Härteprüfungen und Härte. Zeits. Ver. Dt. Ing. 52, 82–85.
Mayo, M.J., Nix, W.D., 1988. A micro-indentation study of superplasticity in Pb, Sn and Sn-38wt%Pb. Acta Metall. 36, 2183–2192.
Menčik, J., Quandt, E., Munz, D., 1997. Determination of elastic modulus of thin layers using nanoindentation. J. Mater. Res. 12, 2475–2484.
Pharr, G.M., Oliver, W.C., Brotzen, F.R., 1992. On the generality of the relationship among contact stiffness, contact area, and elastic modulus during indentation. J. Mater. Res. 7, 613–617.
Raman, V., Berriche, R., 1992. An investigation of the creep process in tin and aluminium using a depth-sensing indentation technique. J. Mater. Res. 7, 627–638.
Sumpter, B.G., Noid, D.W., 1996. On the design, analysis and characterization of materials using computational neural networks. Ann. Rev. Mater. Sci. 26, 223–278.
SNNS, 1995. SNNS Stuttgart Neural Network Simulator, User Manual, Version 4.1. University of Stuttgart, Institute for Parallel and Distributed High Perfromance Systems (IPVR).
Tabor, D., 1951. Hardness of Metals. Cambridge University Press, Cambridge.
Yagawa, G., Okuda, H., 1996. Neural networks in computational mechanics. Arch. Computational Methods Eng. 3, 435–512.